Tectonic controls on the timing of fjord incision at the Antarctic Peninsula

Anna Clinger [a,b,*], Matthew Fox [c], Greg Balco [b], Kurt Cuffey [a,d], David Shuster [a,b,*]

[a] *Department of Earth and Planetary Science, University of California, Berkeley, Berkeley, CA, United States*
[b] *Berkeley Geochronology Center, Berkeley, CA, United States*
[c] *Department of Earth Sciences, University College London, London, United Kingdom*
[d] *Department of Geography, University of California, Berkeley, CA, United States*

ARTICLE INFO

ABSTRACT

We report 534 detrital apatite (U-Th)/He thermochronometric ages collected along a >400 km latitudinal transect along the Antarctic Peninsula (AP). We use the dataset to evaluate the relative roles of climate change and tectonics on the timing of km-scale fjord incision. We find that the onset of km-scale topographic change occurred more than 15 million years after the initiation of glaciation in the region, and generally coincided with the arrival times of the spreading ridge at different latitudes. These results indicate that tectonically-initiated rock uplift accelerated rates of erosion during long glacial conditions at the AP. We infer that rock uplift primarily affected glacial erosion rates by increasing topographic relief, and thereby increasing ice motion and its capacity to erode. These are among the first empirical observations to reveal that a tectonic history, and its control on the regional topography of a landscape, has influenced glacial erosion rates over geologic timescales.

1. Introduction

The advance and retreat of glaciers have played a fundamental role in landscape evolution and sediment transport throughout Earth history. Yet, knowledge of how glacial erosion processes modify topography over million year (Ma) timescales is limited. There are reasons to expect that both climate change (e.g., Alley et al., 2019; Herman et al., 2013; Koppes et al., 2015) and tectonic transitions (Molnar and England, 1990; Raymo and Ruddiman, 1992) can influence glacial erosion processes over million year timescales. However, the hypotheses on how these different forcings can influence rates of glacial erosion have proven difficult to test. This is because few locations on Earth contain sufficiently long records of glacial erosion to have recorded changes in both climate and tectonics. Glaciation in mid-latitudes was initiated synchronously in both tectonically active and inactive regions by Plio-Pleistocene cooling at 2.6 Ma whereas the timescale of major changes in tectonic regime is typically at least several million years. Thus, it is not clear that there are any mountain ranges where the tectonic influence on glacial erosion processes could be

clearly identified from only the Pleistocene glacial record. At high latitudes, however, glacial conditions persisted long enough that the influence of tectonic change on glacial erosion rates may be recorded in geologic records.

The Antarctic Peninsula (AP; Fig. 1a) offers an opportunity to investigate how glacial erosion, climate, and tectonics influenced topography over million year timescales. The AP is a high latitude glacial landscape that has been glaciated since ∼37 to 34 Ma (Anderson et al., 2011) and has since been subject to climate and tectonic change. In particular, the arrival of the spreading ridge, associated with subduction of the Phoenix Plate beneath the Antarctic Plate (Larter and Barker, 1991) (Fig. 2), occurred >15 million years after alpine glaciations initiated. The arrival of the spreading ridge is hypothesized to have caused uplift followed by subsidence (Larter and Barker, 2009). The timing of its arrival and intersection with the trench varied latitudinally (Larter and Barker, 1991). Today, a network of deeply-incised fjords flanks the plateau of the AP and unambiguously demonstrate that glacial erosion processes exerted a first-order control on the topography. An outstanding question is whether the arrival of the spreading ridge influenced fjord incision across the glaciated AP. Exhumation may have been induced by relief development due to tectonics.

In this study, we investigate the relative roles of the arrival of the spreading ridge and contemporaneous climate change on glacial erosion processes across the AP using detrital apatite

---

* Corresponding authors at: Department of Earth and Planetary Science, University of California, Berkeley, Berkeley, CA, United States.
E-mail addresses: aeclinger@berkeley.edu (A. Clinger), dshuster@berkeley.edu (D. Shuster).
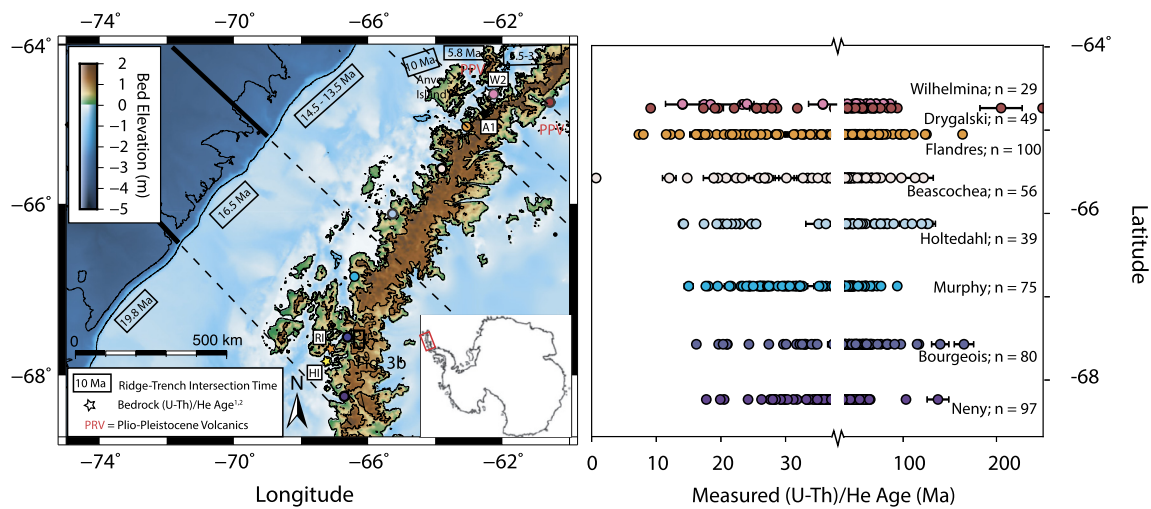
Fig. 1. (Left) Subglacial and submarine topography of study region. Each sample location is indicated by a different color circle, which corresponds to the measured detrital apatite (U-Th)/He data at that site (Right). Major faults are designated by the black solid lines. The dashed lines are extrapolations of the faults to intersect with the AP. Because the spreading ridge intersected with the trench at an almost parallel angle, the latitude of intersection between each dashed line and the AP plateau is used to compare the arrival time of the spreading ridge with each sampling location in Fig. 5. The timing of spreading ridge arrival from Larter and Barker (1991) is annotated in the black text boxes and areas influenced by Plio-Pleistocene volcanics (PPV) are labeled in red text. The bedrock samples are denoted by stars (A1 and W2 = Bedrock sample from Guenthner et al. (2010); RI and HI = Bedrock sample from Clinger et al. (2020)). W2 = Wilhelmina2 (white star), A1 = Andvord1 (black star), RI = Ridge Island (orange star), HI = Horseshoe Island (yellow star). (For interpretation of the colors in the figure(s), the reader is referred to the web version of this article.)
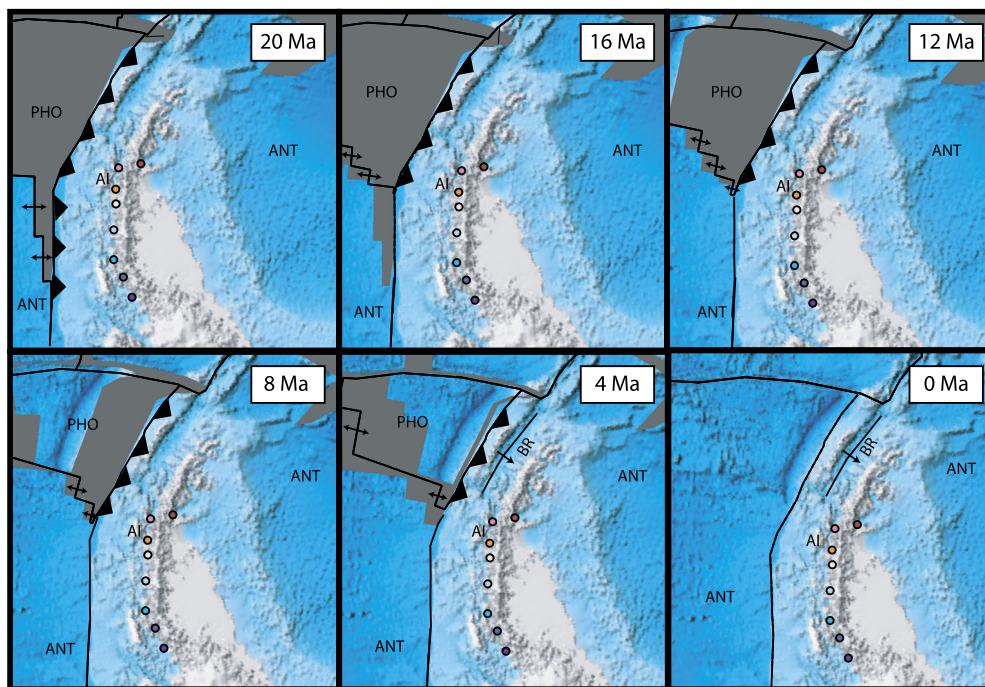
Fig. 2. Tectonic and plate reconstruction of the AP region using GPlates (Müller et al., 2018) since the Neogene. Plate boundaries are shown by black lines. PHO = Phoenix Plate; ANT = Antarctic Plate; AI = Anvers Island; and BF = Bransfield Rift. Sampling sites are depicted with circles and are the same color as in Fig. 1. Spreading ridges are depicted by double arrows. Active subduction is depicted by black triangles. Plate motion over time is visually tracked by modern aerial imagery.

(U-Th)/He (AHe) thermochronometry. We present a new record of 534 detrital AHe ages collected within eight fjords spanning a >400 km latitudinal transect. The AHe ages provide a quantitative constraint on the timescale of exhumation of rocks through crustal temperatures of ∼60 to 90 °C (Reiners and Brandon, 2006), corresponding to ∼1 to 3 km of depth. We use these data to constrain thermo-kinematic models and to quantify the permissible timing and duration of km-scale topographic change across the AP. This approach allows us to evaluate hypotheses on how changes in climate and tectonics initiated erosional responses across glacial landscapes. The results indicate that km-scale topographic change

initiated >15 million years after the onset of alpine glaciations, and generally coincides with the arrival times of the spreading ridge at different latitudes. These results have important implications for understanding how tectonically-driven changes in topography influence glacial erosion rates on geologic timescales.

2. Climate, tectonics, and topography of the Antarctic Peninsula

Because modern ice cover obscures most terrestrial evidence, the glacial response to climate change along the AP is primarily understood through work characterizing offshore sedimentary

records (see review in Davies et al., 2012). The earliest signs of alpine glaciation occur in the sedimentary record drilled offshore the northernmost AP between 37 to 34 Ma (Anderson et al., 2011). This finding is supplemented by a few accessible terrestrial records of glaciation at the AP that date to at least the Oligocene (Davies et al., 2012). From ~34 Ma to ~9 Ma, the AP glacial record is poorly constrained, but some information about characteristics of glaciation is available from the discontinuous offshore records (Anderson et al., 2011), which have depositional ages of 28.4 to 23.3 Ma and 12.8 to 11.7 Ma. An increase in pebble counts and a reduction in pollen counts is observed in these cores over this timeframe, which has been used to support ice sheet expansion prior to ~12 Ma and in response to Miocene cooling (Anderson et al., 2011). This interpretation is consistent with the timing of inferred change in glacial dynamics across Antarctica (e.g., Flower and Kennett, 1994; Spector and Balco, 2021; Zachos et al., 2001).

The longest continuous records of AP glaciation are located along the western continental margin and extend to ~9 Ma (Barker and Camerlenghi, 2002). These records reveal that the ice sheet has repeatedly advanced across the continental shelf since 9 Ma and with increased frequency since the Pliocene (e.g., Bart and Anderson, 2000). Limited terrestrial records suggest the advanced margin of the ice sheet was never more than ~850 m thick during glacial maxima (Smellie et al., 2009). In response to Pleistocene cooling at ~3 Ma, a transition from polythermal to cold-based ice has been inferred by a regional change in western AP shelf architecture and a decrease in sedimentation rates (Rebesco et al., 2006).

Tectonic events at the AP over the last 200 million years are reviewed in Jordan et al. (2020). In summary, the AP is a continental margin magmatic arc with a long history of subduction and related magmatism. A summary of the regional geology is shown in Fig S1. For more detailed geologic information, the reader is referred to https://data.gns.cri.nz/ata_geomap/index.html?map=Antarctic (Cox et al., 2019). The earliest magmatism dates to the early Ordovician, with peak arc volcanism in the Jurassic to Cretaceous period (Jordan et al., 2020). The transpressional Palmer Land Event caused widespread deformation at ~107 to 103 Ma (Vaughan and Storey, 2000). With the exception of the Bransfield Strait region, subduction stopped between ~20 – 4 Ma (Larter and Barker, 1991), after the spreading ridge between the subducting Phoenix Plate and the Antarctic Plate intersected the trench along the western AP margin. The ridge-trench intersection migrated to the north between 20 to 4 Ma (Fig. 2). A slab window is hypothesized to have opened in response to this intersection (Breitsprecher and Thorkelson, 2009).

Tectonism is hypothesized to have led to surface uplift of the high elevation plateau that spans the spine of the AP (Elliot, 1997). The timing of surface uplift is poorly constrained. The favored hypothesis is that the arrival of the spreading ridge in the Neogene triggered rock uplift of a low-relief landscape (Elliot, 1997). Rock uplift may have occurred in response to the formation of the slab window behind the subducting plate and subsequent upwelling of the asthenosphere (Breitsprecher and Thorkelson, 2009), increased shortening and generation of a thickened crustal welt in response to coupling between the migrating spreading ridge and the overriding Antarctic Plate (e.g., Furlong and Govers, 1999; Stevens Goddard and Fosdick, 2019), or large-scale dynamic topography (Guillaume et al., 2013). Transient thermal uplift, and subsequent subsidence, may have occurred in response to the opening of the slab window (Larter and Barker, 1991). An alternative but not exclusive hypothesis is that rock uplift occurred in the Late Cretaceous at ~100 to 85 Ma and in response to a decrease in spreading rates along the Phoenix and Antarctic Plate boundary (Elliot, 1997) and/or terrane accretion during the Palmer Land Event (Guenthner et al., 2010). In this case, Neogene tectonics may

not have generated additional km-scale relief. Low-temperature thermochronometric ages of AP bedrock located along the coast reveal a latitudinal difference in exhumation that supports both hypotheses (Guenthner et al., 2010); both events may have triggered a phase of rock uplift. At latitudes south of Anvers Island (Fig. 1a), increased exhumation in the Miocene is hypothesized to relate to the arrival of the spreading ridge. At latitudes north of Anvers Island, increased exhumation in the Late Cretaceous, and not the Miocene, is inferred. The latitudinal difference is thought to relate to the northward migration of the intersection between the spreading ridge and the trench, and a change in slab geometry between 9 and 6 Ma (Larter and Barker, 1991) that prevented the opening of a slab window at latitudes north of Anvers Island (Guenthner et al., 2010). Geophysical considerations and analogy to similar tectonic environments elsewhere (Furlong and Govers, 1999; Stevens Goddard and Fosdick, 2019) support the hypothesis that the trench-ridge collision drove time-transgressive rock uplift in the Peninsula region. To summarize, tectonic reconstructions propose several possible periods of rock uplift, which may have generated topographic relief and therefore initiated exhumation due to surface erosion.

3. Methods

AHe thermochronometry provides quantitative constraints on the thermal history of rock as it approaches Earth's surface during exhumation (Reiners and Brandon, 2006). ^{4}He is produced by α-decay of uranium and thorium within minerals, but will diffuse out of the crystal at sufficiently high temperatures. In apatite, ^{4}He is quantitatively retained once rocks cool to ~60 – 90 °C (corresponding to ~1 – 3 km of depth), which means the system is sensitive to shallow temperature perturbations due to evolving topography. In turn, bedrock thermochronometric ages can be used to constrain the exhumation rate history of an area. In detrital thermochronometry, the distribution of measured ages relates to the bedrock age distribution in the upstream catchment area and the modern patterns of sediment sourcing across the catchment. Therefore, the detrital ages, combined with other key observations (e.g., the range of ages), can be used to constrain long-term patterns of exhumation. This study uses the framework presented in Clinger et al. (2020), where we applied detrital AHe thermochronometry to constrain the timing of topographic change at Bourgeois Fjord, AP. In that study, we showed that the youngest observed ages at each site are the key observables used to constrain the timing of km-scale topographic change (Clinger et al., 2020). The use of the youngest detrital AHe age to constrain the timing of topographic change is justified because (i) most source rocks are igneous (Fig. S1), and thus the scatter is expected to be small, (ii) there is <2.5 Ma difference between the youngest two AHe ages at the sites with the largest detrital sample size (i.e., Flandres and Neny) suggesting that a smaller sample size will sufficiently sample the youngest age if we assume similar spatial patterns of sediment sourcing, and (iii) there is <5 Ma difference in the youngest age population at all sites except Beascochea and Drygalski (Fig. S2), and (iv) similar latitudinal pattern in the youngest age population at all sites (Fig. S2). Due to the third reason and because it is >7 Ma younger than any other age in the entire dataset, the youngest age at Beascochea is considered an outlier. It is unclear whether the youngest age at Drygalski is anomalous. However, classification of that age as an outlier does not affect interpretations, because we have already identified that results at Drygalski are anomalous (Section 4.1). We summarize the field, analytical, and numerical methods below, as well as several key modifications from the approach used in Clinger et al. (2020). Uncertainties are described extensively in Clinger et al. (2020) and summarized in Supplementary Material Section 1–3.
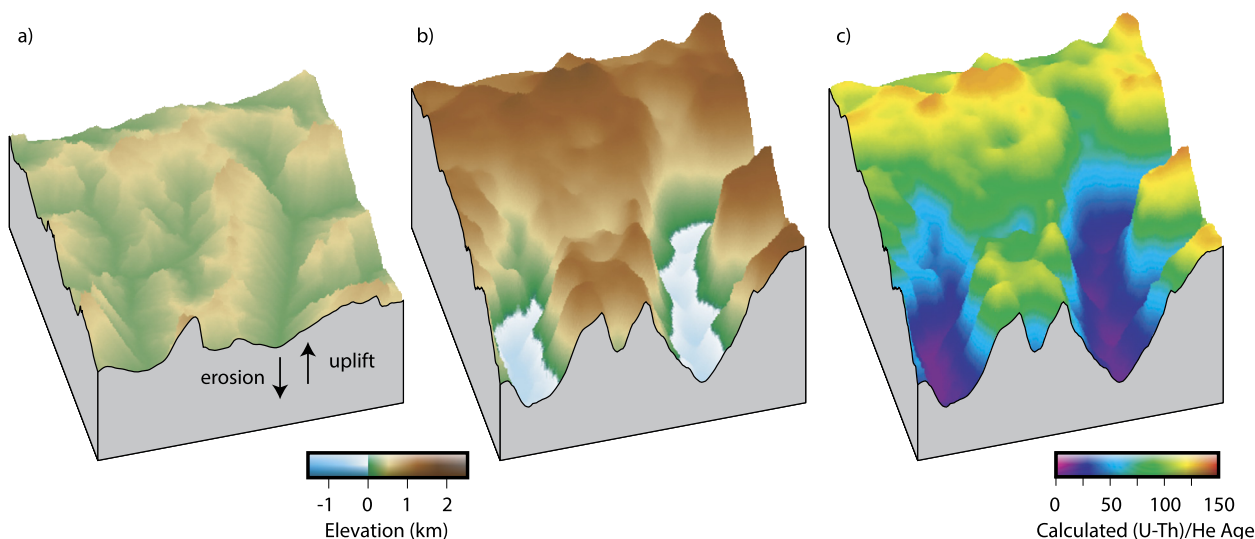
Fig. 3. Example of how the topographic evolution is prescribed in Pecube. Location is Bourgeois Fjord and is designated by box in Fig. 1. a) Preferred pre-glacial landscape constructed following Fox (2019). b) Modern bedrock topography calculated by Huss and Farinotti (2014). c) Calculated apatite (U-Th)/He ages as output from Pecube.

In cruises between 2015 and 2017, we collected box cores from eight fjords located between -64 to -69°S (Fig. 1b). Because the box core penetrated ∼50 cm of sea floor and modern sedimentation rates range from ∼1-10 mm yr^{-1}, we estimate depositional ages of <1 ka (Clinger et al., 2020). We sampled as close to the glacial calving front as ice conditions permitted to reduce uncertainty in sediment sourcing. The apatite crystals were isolated using standard hydrodynamic, magnetic, and density techniques at the Berkeley Geochronology Center. Individual apatite crystals were then handpicked to avoid visible inclusions, weathering, and damage. Some broken crystals were analyzed to increase the sample size. The abundances of U, Th, and He for each crystal were analyzed using standard isotope dilution techniques using multicollector inductively coupled plasma and quadrupole mass spectrometers housed at the Berkeley Geochronology Center. Complete analytical details including our treatments of blanks and standards and additional information on laboratory methods are described in Tremblay et al. (2015). All crystals had a minimum dimension of 60 μm and a standard correction for alpha-ejection losses (F_T) was applied. Sample size varies between each site due to differences in the amount of datable apatite in each box core.

To interpret thermochronometric data in terms of topographic hypotheses, we used the 3D finite element thermo-kinematic code Pecube (Braun, 2003). Pecube solves the heat equation as rock exhumes to Earth's surface and the topography evolves. Material points are tracked through the evolving thermal field and the resulting time-temperature pathways are used to calculate AHe ages across the modern bedrock surface (Fig. 3c), using diffusion kinetics from Farley (2000). The modern bedrock surface was calculated by subtracting calculated ice thicknesses (Huss and Farinotti, 2014) from modern surface elevations (Fig. 3b). We use the numerical modeling approach presented in Fox (2019) to construct our preferred pre-glacial landscape (Fig. 3a and S3). In summary, the modern plateau is interpreted as a relict surface that was once situated near sea level, then uplifted by tectonic processes, and has undergone essentially no glacial erosion. The relict surface was selected from the modern bedrock DEM and used to reconstruct a fluvial landscape consistent with geomorphic scaling laws (Fox, 2019). Another pre-glacial landscape is used in a sensitivity analysis in the supplementary material. In this scenario, the pre-glacial landscape is flat, and set to an elevation such that no exhuma-
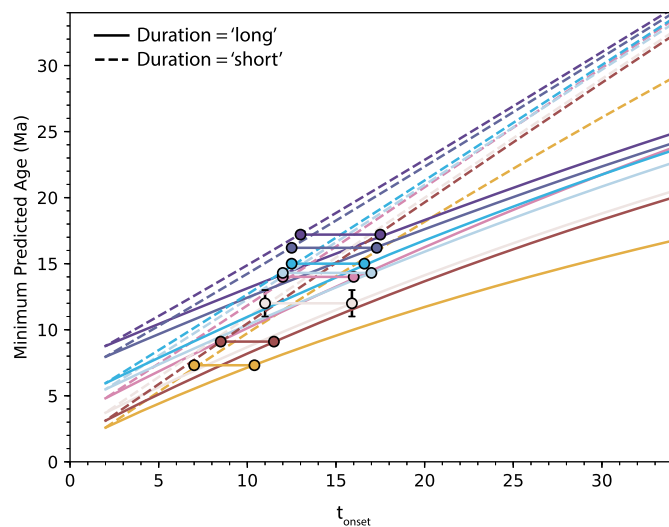
Fig. 4. Summary of numerical modeling results from Pecube. The minimum predicted minimum age is shown as a function of the modeled onset of major topographic change (t_{onset}) at each site assuming a 'short' (2 Ma; dashed) or 'long' (t_{onset} to today; solid) duration of topographic change. Line colors are the same as the color used for each site in Fig. 1.

tion occurs along the highest reaches of the plateau. Because this typically leads to more valley exhumation, the calculated onset of topographic change is earlier by 0 to 6 Ma than in the preferred pre-glacial landscape (Fig. S4 and Supplementary Material Section 3). These differences are ultimately not resolvable by the data. This scenario likely represents the upper limit of the amount of valley exhumation since the onset of major topographic change, given the plateau form of all the modern residual topography between the fjords.

The timing of these changes is controlled by a key input parameter: the onset time of km-scale topographic change, which we define as t_{onset}. In Pecube, we vary t_{onset} from 34 to 2 Ma to test different hypotheses of how t_{onset} relates to climate and tectonic change. Changing the t_{onset} primarily affects the minimum observed ages that are located at the valley fjord (Fig. 3c). Each value of t_{onset} is determined by selecting the model that most closely predicts the youngest measured age in each catchment (see Fig. 4). We also investigate how the choice of a short
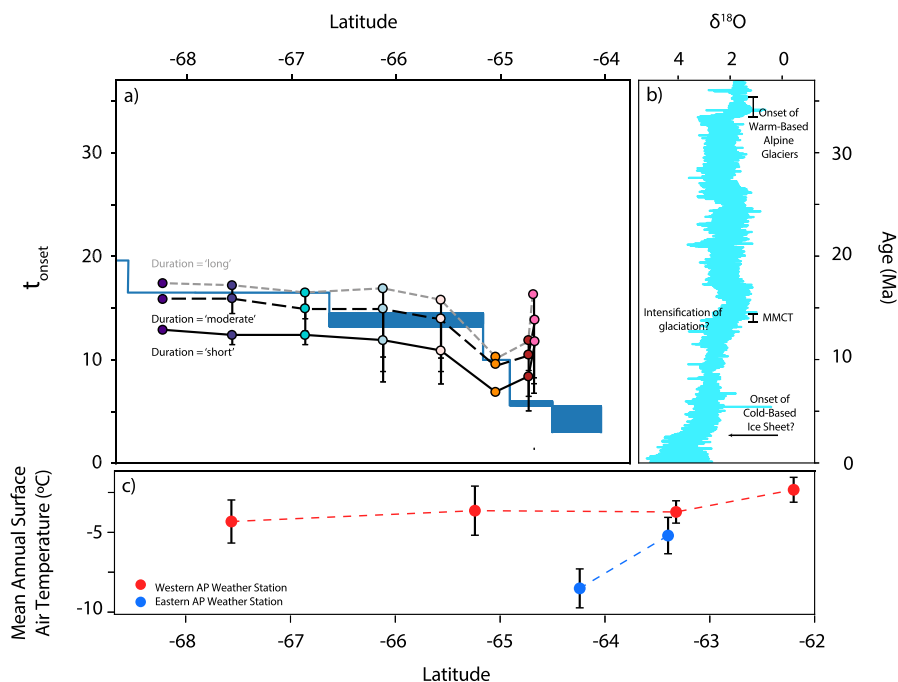
Fig. 5. Relationship between the timing of topographic, climate, and tectonic change at the AP. a) Calculated onset of major topographic change (t_{onset}) from Pecube at each site assuming the duration of topographic change is 'short' (2 Ma; solid, black line), 'moderate' (t_{onset} to 3 Ma; dashed, black line), and 'long' (t_{onset} to today; dashed, grey line). The colors used for each fjord are the same as in Fig. 1. Estimated uncertainty related to sediment sourcing is shown by the error bars (see Section 4.1). Latitudinal variation of the timing of spreading ridge arrival is shown by the solid blue lines. Uncertainty in the arrival time is shown by the line thickness. The latitude of arrival corresponds to where the dashed line in Fig. 1 intersects with the AP plateau. b) Global climate change as revealed by benthic δ^{18}O (Zachos et al., 2001). The inferred timing of major glacial events along the AP is annotated. MMCT = Mid-Miocene Climate Transition. c) Mean annual surface air temperature from eastern (blue) and western (red) AP weather stations from 1951 to 2014 (Turner et al., 2016).

(2 Ma; defined as 'short') and long, steady duration (from t_{onset} to today; defined as 'long') of topographic change affect interpretations. We also include a scenario of steady exhumation from t_{onset} to 3 Ma, which is the hypothesized time that cold-based ice established along the AP (Rebesco et al., 2006) (defined as 'moderate'). In all scenarios, a background exhumation rate of 0.01 km Ma^{-1} is used and the model starts at 180 Ma. We describe key model parameters in the Supplementary Material Section 1. Calculated valley exhumation rates range from 0.9 to 1.7 km Ma^{-1} and from 0.1 to 0.2 km Ma^{-1} for a 'short' and 'long' duration of km-scale topographic change, respectively. Using our preferred modeling parameters and assumptions, the range of t_{onset} at each site is less than 4 Ma at all sites. We discuss how the assumptions may affect uncertainty in t_{onset} in Supplementary Material Section 3. We also assume methodological biases are approximately the same at all sites. If this is a valid assumption, latitudinal variation in t_{onset} is not an artifact of our modeling approach (Supplementary Material Section 3).

4. Results

We report 534 detrital AHe ages in Fig. 1 and Table S1-9. At all sites, we observe >70 Ma of difference between the oldest and youngest AHe ages. We also find a northward, systematic decrease in the youngest measured AHe ages; from Neny Fjord (18 Ma; n = 97) to Flandres Bay (7 Ma; n = 100). Then, the two northernmost sites (north of 64.75°S), Drygalski (n = 49) and Wilhelmina (n = 29), have slightly older minima of 9 and 14 Ma, respectively. The oldest AHe ages of all sites vary between 85 to 298 Ma and generally the age distributions all have long-tailed distributions. These distributions are likely due to the presence of cold-based ice along the high-elevation plateau, which suppresses modern sediment sourcing from regions expected to have oldest AHe ages in

the landscapes (Clinger et al., 2020). We find no latitudinal pattern in the oldest measured AHe ages.

The best-fitting onset times of km-scale topographic change, t_{onset}, range from 16 to 7 Ma (Fig. 5 and Table S10). This is notable because in all models the best-fitting values of t_{onset} are more than 15 Ma after the supposed onset of alpine glaciation. Latitudinal variation in the calculated t_{onset} generally covaries with the latitudinal variation in the minimum measured AHe age. South of Anvers Island (>64.75°S), we find the data are best explained by models with a t_{onset} that is approximately equal to the arrival time of the spreading ridge at each site; the best-fitting onset times, t_{onset}, range from 13 to 7 Ma assuming a 'short' duration of topographic change and 16 to 10 Ma assuming a 'moderate' duration of topographic change. In the latter scenario, the assumed duration of topographic change thus varies between sites, from 13 to 7 Ma. Scenarios assuming a 'long' duration of topographic change are excluded using offshore geologic records (Supplementary Material Section 2). At latitudes north of Anvers Island, we find best-fitting models of t_{onset} are earlier than the arrival time of the spreading ridge and range from 9 to 17 Ma. However, we note that one of these sites (Wilhelmina) has a small sample size (n = 29) and the other (Drygalski) is located on the eastern AP. 'Short' and 'moderate' durations of topographic change lead to calculated valley incision rates of 0.1 – 1 km Ma^{-1}. These rates are comparable to rates of glacial erosion across the globe on centennial to million year timescales (e.g., Koppes and Montgomery, 2009). The predicted age-elevation profiles agree with the few bedrock AHe ages that have been reported in the literature (Guenthner et al., 2010; Clinger et al., 2020) and located in comparable sites (Fig. 6). In the Wilhelmina comparison, we note that the bedrock sample Wilhelmina2 was located in the outer bay (~0 m asl), whereas our sample site was located in the inner bay. The bedrock sample Andvord1 was located in the inner bay (~0 m asl), but in the
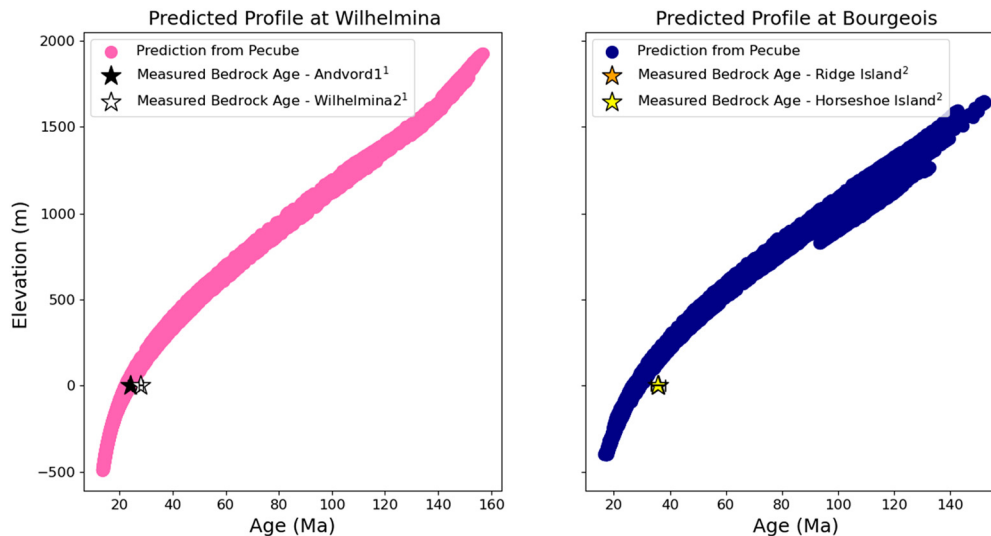
Fig. 6. Comparison between predicted age-elevation profile from Pecube at Wilhelmina (Left) and Bourgeois (Right). The age-elevation profiles are the results from the preferred pre-glacial landscape. The predicted results are shown for both a 'short' and 'moderate' duration of topographic change. The locations of the bedrock samples are shown in Fig. 1. 1 = Guenthner et al., 2010; 2 = Clinger et al., 2020.

fjord directly south of our sample site. In the Bourgeois comparison, the bedrock samples are also located in the outer bay while our sample site is located in the inner bay. Thus, differences in the exhumation history of the bedrock samples may exist.

4.1. Uncertainty related to detrital sample size

A key source of uncertainty relates to sample size (n). The concern here is that the minimum AHe age (a_{min}) that actually exists in the landscape may not have been sampled due to a small sample size. Because the measured a_{min} is used to determine t_{onset}, t_{onset} may be biased to older values. To obtain an estimate of the uncertainty in t_{onset} related to sample size, we use a simple Monte Carlo bootstrap approach. In summary, we constructed an artificial distribution of ages, with a known, synthetic, a_{min}, and then repeatedly sampled it a number of times, n, to calculate the probability of sampling each age. We then calculated the probability of sampling the true a_{min} for a given number of detrital ages. This allowed us to estimate how much older our measured a_{min} is compared to the true unknown a_{min} in the landscape. We also calculated the difference between the true a_{min} and the sampled a_{min} for a given n. Then, we combined this information with the calculated relationship between t_{onset} and the sampled a_{min} at each site (Fig. 4) to assign an uncertainty to each t_{onset}. We describe these steps in detail below.

First, we constructed an artificial distribution of ages. The expected difference between a true a_{min} and the measured a_{min} is a function of this distribution. At each site, the distribution of ages depends on patterns of sediment sourcing and the spatial distribution of ages, which are both unknown in this study. In order to ensure that the artificial distribution was similar to the true distribution, we decided to use the measured distribution of ages at sites with sufficiently large sample sizes (n > 50). We explicitly assumed that patterns of sediment sourcing and the spatial distribution of ages at each site were similar. This is likely not true in reality. We linearly scaled each measured distribution with n > 50 to a chosen true a_{min} (e.g., 5 Ma). Because of the large range of ages at each site, the choice of true a_{min} did not substantially affect uncertainty estimates as long as a_{min} is relatively young (e.g., <10 Ma). Next, we combined all scaled distributions to construct one artificial distribution of ages. This is the distribution of ages that will be sampled to obtain uncertainty in t_{onset} at each site.
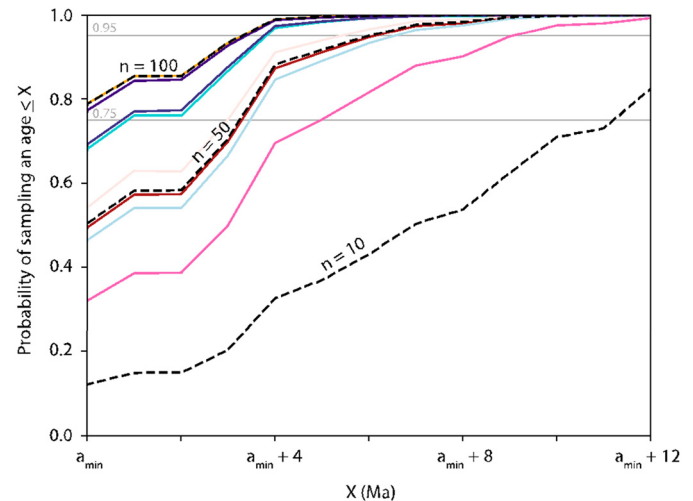
Fig. 7. Results from Monte-Carlo bootstrap approach to assessing uncertainty in the measured minimum age (a_{min}) at each site due to sample size (n). The probability of sampling an age greater than or equal to a given age (X Ma) is shown for each integer greater than the synthetic a_{min} for a number of different n. If n = 50 grains, there is a probability of ∼0.75 of sampling within 3 Ma of the synthetic a_{min}. Each line corresponds to a different site and uses the same color scheme as in all previous figures. This calculation is described in Section 4.1.

The artificial distribution of ages was then sampled n times to obtain a 'sampled distribution'. This exercise was repeated 10,000 times. The probability of sampling true a_{min} was calculated by counting the number of sampled distributions that sampled a_{min} divided by the total number of sampled distributions. This calculation was repeated for all integers greater than the true a_{min}. The results for each sample size in this study are shown in Fig. 7. Using this information, we determined which age corresponds to the 0.75 probability of inclusion in the sampled distribution for a given sample size. We note that this uncertainty only lowers t_{onset}, because the measured a_{min} is the upper limit of the true a_{min}. Then, we used the relationship between t_{onset} and the predicted a_{min} in Pecube at each site (summarized in Fig. 4) to determine which value of t_{onset} corresponds to this new lower limit of a_{min} at each site and for each duration of topographic change. These new lower limits are the uncertainty bars shown in Fig. 5. The uncertainty ranges from ∼8 Ma at Wilhelmina assuming a 'long' duration of

topographic change and ∼0 Ma at Neny assuming a 'short' duration of topographic change.

To illustrate this calculation, we used Wilhelmina as an example. Wilhelmina has a sample size of 29 and a measured a_{min} of 14.1 Ma. In Fig. 7, the probability of sampling each age with n = 29 is shown by the pink line. From inspection, we observed that the probability of measuring an a_{min} that is 5 Ma older than the true a_{min} (i.e., amin + 5) is about 0.75. This means that there is a 0.75 probability that the true a_{min} at Wilhelmina was >9.1 Ma. If a_{min} at Wilhelmina is 9.1 Ma, the calculated t_{onset} is ∼7 Ma if the duration of topographic change is 'short' and ∼8 Ma if the duration of topographic change is 'long'. These values are ∼5 and ∼8 Ma lower than the calculated values of t_{onset} and are the lower limits shown in Fig. 5a.

Considering these uncertainties, it is plausible that t_{onset} at Wilhelmina and Drygalski was similar to the arrival time of the spreading ridge. However, we note that the youngest age at Drygalski may be an outlier (Fig. S2), which would argue against this interpretation. Another conclusion is that t_{onset} is still >10 Ma after the onset of glaciation and before 3 Ma at all sites when sample size uncertainty is considered.

5. Discussion

Because the oldest measured AHe ages are at least as old as Late Cretaceous tectonism and the youngest measured AHe ages are younger than the onset of glaciation at the AP at each site, we infer that the km-scale topographic relief observed today was primarily generated by valley incision by glaciers. The >70 Ma range of AHe ages at each site strikingly demonstrates how spatially variable long-term exhumation rates can be across glacial landscapes. Since the onset of glaciation, each site is characterized by >2 km of exhumation in the valleys and most likely less than several 100's of m of exhumation along the high-elevation plateau.

To evaluate the relative influence of climate and tectonics on the timing of incision at each latitude, we compare the best-fitting values of t_{onset} (Fig. 5) to independent records of regional climate, sedimentation and tectonics to test the following four hypotheses on what controlled the timing of km-scale topographic change: (i) the initiation of alpine glaciation, (ii) the subsequent intensification of glaciation due to progressive cooling, (iii) tectonically-initiated rock uplift, or (iv) coupling between progressive cooling and uplift initiated km-scale topographic change. We find that the tectonically-initiated rock uplift hypothesis best explains the timing of accelerated topographic change at the AP.

5.1. The role of climate and tectonics on the timing of topographic change

Progressive cooling from a fluvial to a polar-glacial climate can influence erosion in several ways. First, the onset of glaciation initiates a transition from solely fluvial to glacial erosion processes, and in some cases such transition is known to have accelerated exhumation (e.g., Haeuselmann et al., 2007; Herman et al., 2013; Willett et al., 2020). In our preliminary work characterizing t_{onset} at a single fjord at the AP (Clinger et al., 2020), the best-fitting values of t_{onset} ranged from 30 to 12 Ma, which led us to infer that exhumation increased in response to the initiation of alpine glaciation at the AP. However, with the addition of the new data and the quantitatively reconstructed pre-glacial landscape presented here, we find that best-fitting values of t_{onset} at all sites occur more than 15 Ma after the supposed onset of alpine glaciation. Thus, the switch from fluvial to glacial conditions alone cannot have initiated km-scale topographic change here.

As the climate continued to cool, two counteracting influences might have governed glacial erosion rates. Progressive cooling can

reduce the amount of surface melt, which in turn reduces glacial erosion by allowing sediment to accumulate at the glacier bed and protect the bed from further erosion (e.g., Alley et al., 2019). Today, comparison of sediment yields from tidewater glaciers in Patagonia and the AP clearly highlights the effect of reduced surface melt on suppressing subglacial erosion rates at higher, colder latitudes (Koppes et al., 2015).

On the other hand, a cooling climate also leads to an expansion of ice cover across the landscape and increased ice flux, which would likely increase erosion. This process can even involve greatly increased erosion through positive feedback between topography, steering of ice flow, ice velocity, and erosion (Kessler et al., 2008). Implicit in this relationship are changes in precipitation, which depend on changes in climate and orography and control ice fluxes. The combined effect of meltwater and expansion suggests that a maximum of glacial erosion rates will be achieved as the climate cools and perhaps well after onset of glaciation. We expect this maximum to have occurred while surface melt remained abundant and prior to sufficient cooling to transform glaciers into polythermal and, ultimately, polar thermal states. Thus, a second hypothesis is that peak glacial erosion rates occurred in the Miocene, which is defined by a period of progressive cooling.

At all sites, there is a permissible t_{onset} during the Miocene (Fig. 5a and b). While we cannot discount that progressive cooling in the Miocene accelerated glacial erosion rates entirely, it does not explain the observed latitudinal trend in t_{onset}, a feature of our data that emerges whether we assume a duration of topographic change is 'short', 'moderate', or 'long' (Fig. 5a). Modern surface air temperatures only vary by ∼ 1°C from 67.5°S to 63.5°S on the western AP (Turner et al., 2016) (Fig. 5c), a consequence of shore-parallel ocean currents. Thus, no latitudinal trend in climate is likely to covary with our inferred t_{onset}. While spatial patterns of surface air temperature may have been different in the past, differences would most likely arise due to changes in the size and shape of land masses in response to tectonically-initiated rock uplift, and not progressive cooling. With the information at hand, we conclude Miocene progressive cooling may have helped accelerate glacial erosion rates, but progressive cooling alone did not initiate km-scale topographic change along the AP.

Since the best-fitting values of t_{onset} correlate closely with the arrival time of the spreading ridge at sites south of Anvers Island (Fig. 5a), the arrival of the spreading ridge during glacial conditions may have somehow accelerated km-scale topographic change. One hypothesis is that northward migration of the spreading ridge and trench intersection between ∼20 to ∼4 Ma induced a northward progression of uplift (Guenthner et al., 2010), which in turn increased glacial erosion rates. Assuming a 'short' duration of topographic change, t_{onset} lags the arrival time of the spreading ridge by ∼3-5 Ma; assuming a 'moderate' duration of topographic change, t_{onset} is within a few million years of the arrival time of the spreading ridge. These results strongly suggest that tectonics controlled the timing of km-scale topographic change at these sites.

At the two sites north of Anvers Island (Wilhelmina and Drygalski), the synchroneity breaks down. Here, t_{onset} predates the arrival time of the spreading ridge (i.e., by 3 to 7 Ma and by 5 to 8 Ma assuming a 'short' and 'moderate' duration of topographic change, respectively). These two sites are located at latitudes where the spreading ridge arrives more recently than 10 Ma. Thus, the hypothesis that tectonic change drove glacial valley incision cannot entirely explain our dataset. It is possible our observations at the two northernmost sites are spurious due to undersampling of the detrital AHe ages, as shown by the error bars in Fig. 3. However, Guenthner et al. (2010) observed a similar shift to older bedrock AHe ages at latitudes north of Anvers Island. Their use of bedrock samples suggests the change in the relationship between the ar-

rival of the spreading ridge and t_{onset} at sites north of Anvers Island is not entirely related to a sampling bias. They proposed that rotation of the slab during subduction between 9 and 6 Ma (Larter and Barker, 1991) prevented the slab window from migrating north of Anvers Island and consequently affected exhumation rates. However, no systematic difference in glacial geomorphology or in the reconstructed amount of valley exhumation since t_{onset} (Table S10) is observed at the two northernmost sites. Hence, there are aspects about the relationship between tectonics and valley incision at the AP that we do not fully understand. A more complex relationship at the two northernmost sites may be the consequence of rifting in the Bransfield Strait region or progressive cooling throughout the Neogene. Ultimately, additional work is required to understand why t_{onset} predates the arrival time of the spreading ridge at the two northernmost sites.

5.2. Tectonic controls on glacial erosion rates

While glacially-carved landscapes are often associated with a cooling climate, our results indicate that tectonically-initiated rock uplift generally accelerated km-scale incision >15 Ma after the onset of glaciation at the AP. We suggest that rock uplift influenced glacial erosion rates by increasing range elevation and generating topographic relief, which leads to locally, and regionally, higher slopes. There are at least two reasons why higher slopes would increase glacial erosion rates. Both relate to the fact that, all else being equal, glacial erosion is expected to increase with the rate of sliding motion (Alley et al., 2019). First, a higher slope causes the ice to be thinner for a given ice flux, which increases the rate of motion (Shuster et al., 2011). Second, a higher slope increases orographic precipitation and hence ice flux, which must be accommodated by faster motion (Anderson et al., 2006). Another way tectonics can influence erosion rates is through fracturing of bedrock during deformation and unloading (Molnar et al., 2007). Glacial quarrying rates are known to increase with the abundance of pre-existing fractures (Dühnforth et al., 2010). These effects can be amplified by ice sheet loading effects across glacial cycles (Leith et al., 2014) and the effects of co-eval climate change on ice flux.

Because glaciers require land above sea level to nucleate, surface uplift can also initiate glacial erosion by simply elevating rock above sea level. This effect could potentially explain why km-scale topographic change occurred >15 Ma after the initiation of glaciation and covaries with the arrival time of the spreading ridge. Evidence indicates, however, that at least part of the pre-glacial landscape was situated above sea level after the onset of glaciation, with the limited offshore sedimentary records suggesting (i) terrigenous sedimentation since at least 34 Ma (Anderson et al., 2011; Rebesco et al., 1997) and (ii) the AP hosted a tundra landscape with woodland vegetation in the Eocene (Anderson et al., 2011). On the other hand, we cannot be certain that the subaerial landscapes contributing to these records coincided with the modern plateau regions.

Another consequence of tectonic change via subduction is magmatism in the forearc region. Thus, one question is whether the youngest AHe ages relate to magmatism, and not the timing of km-scale topographic change. While we cannot completely rule out this hypothesis, the similarity in range and shape of the distribution of ages between our different sites suggests that this is unlikely. Magmatic flare-ups would likely be randomly distributed within the catchment, inducing dissimilarity in the age distributions between sites. This is because the shape of the distribution of ages is controlled by both the spatial distribution of ages and patterns of modern sediment sourcing at the AP (Clinger et al., 2020).

If we accept that time-transgressive ridge-trench interaction was, in fact, accompanied by surface uplift, then our results are

significant as among the first empirical results indicating that tectonism influences glacial erosion rates by modifying topography, in the context of a decades-long effort to constrain the relationship between glaciers, climate, tectonics, and topography (e.g., Molnar and England, 1990; Oerlemans, 1984; Pedersen and Egholm, 2013). Our results are consistent with one expected relationship between topography and glaciers; increased topographic relief increases ice motion due to steeper slopes and greater accumulation, and thus enhances glacial incision. The enhanced rate of incision could be temporary, however. Modeling studies have also found negative feedback between topography and ongoing glacial erosion (Egholm et al., 2009; Oerlemans, 2002; Pedersen and Egholm, 2013; Shuster et al., 2011), because erosion can remove enough rock to reduce elevations in the catchment sufficiently to reduce accumulation. Together, our results and previously published modeling results indicate a potentially complex relationship on geologic timescales between glacial erosion rates and topography evolving in response to both tectonics and glaciation.

5.3. Glacial erosion processes during the first 15 million years of glaciation

One important question raised by our results is the following: why did the first >15 Ma of glaciation not initiate km-scale topographic change at the AP? One interpretation, as noted previously, is that the low-relief landscape now constituting the plateau was below sea level and largely unoccupied by ice. A second interpretation is that glacial erosion is simply not effective on a low-relief surface such as the one that prevailed here prior to tectonic uplift. If so, our results reveal that the initiation of glaciation alone does not always lead to accelerated erosion. Conversely, if significant topographic relief was produced by tectonic rock uplift prior to glaciation, the initiation of glaciation can renew km-scale topographic change. Fennoscandia provides an example of this scenario. While that landscape has been tectonically inactive since long before the regional onset of glaciation in the Pleistocene, preglacial tectonism led to the development of broad extensional valleys across western Fennoscandia and influenced patterns of glacial erosion (e.g., Osmundsen et al., 2010). The most dramatic example is perhaps illustrated at Sognefjord, Norway. Here, it has been proposed that ice preferentially flowed along zones of rock-structure weakness, generated by tectonism, and carved the >1 km below sea level overdeepening (Nesje and Whillans, 1994).

A third interpretation is that the locus of exhumation moved from west to east over time. If the pre-glacial mountain range was broader in the east-west direction prior to the initiation of glaciation, glacial erosion may have been previously focused along the western flanks of the pre-glacial mountain range, and not where the fjords are located today. Thus, the topography that developed during the first 15 Ma of glacial conditions may have been completely eroded by the time the spreading ridge intersected with the trench. This hypothesis may also help reconcile some enigmatic aspects of the geomorphology of the AP. Every subduction zone on this planet is associated with some kind of mountain range; yet, the AP is characterized by its broad plateau deeply incised by glaciers. In this scenario, it is possible that the axis of the mountain range was situated to the east or west of the current peninsula and subsequently eroded. One observation that argues against this interpretation is that no glaciers on the western AP have eroded through the plateau and breached the drainage divide. Breached divides are observed across many glacial landscapes (e.g., Alaska, the Cascades, Patagonia, Norway) and are associated with headward propagating erosion. Additionally, if the locus of exhumation moved from west to east over time, we predict t_{onset} and/or the duration of topographic change should systematically relate to the distance from the shelf edge as measured down a glacial flowline.

Latitudinal variation in flowline distance to the shelf edge argues against this explanation. For example, the flowline distance from Bourgeois to the shelf edge is larger than the flowline distance of either of its neighboring fjords (Neny and Murphy), yet t_{onset} gradually decreases from Neny to Murphy. Nonetheless, more-complex spatial and temporal patterns of exhumation since the onset of glaciation might explain these enigmatic observations. These hypotheses warrant further investigation, as they have important implications for understanding the efficacy of glacial erosion on geologic timescales. Importantly, testing this hypothesis would require collected bedrock material from locations that are currently under the sea.

6. Conclusions

In this study, we found that km-scale topographic change accelerated more than 15 million years after the initiation of glaciation at the AP, most likely in response to the arrival of a spreading ridge. Although the exact process by which ridge-trench interactions generated surface uplift is not precisely known, the temporal association between the onset of exhumation and hypothesized northward-propagating surface uplift indicates that such uplift likely occurred and that increased glacial erosion rates were likely a consequence of increased topographic relief generated by tectonically-initiated rock uplift. These results reveal how topography, when modified by tectonics, can influence glacial erosion rates on geologic timescales. The results also demonstrate that the onset of glacial conditions alone do not necessarily enhance erosion rates, though further constraints on regional history are needed to interpret this conclusion. The ability to identify a tectonic control on glacial processes is an important advance needed to inform numerical models of glaciations and long-term glacial erosion. Records of tectonic change and paleogeography may have particular utility for evaluating hypotheses about how glaciers shaped Earth's surface on geological timescales.

CRediT authorship contribution statement

Anna Clinger: Formal analysis, Investigation, Methodology, Visualization, Writing – original draft. **Matthew Fox:** Formal analysis, Investigation, Methodology, Writing – review & editing. **Greg Balco:** Conceptualization, Funding acquisition, Investigation, Methodology, Writing – review & editing. **Kurt Cuffey:** Investigation, Methodology, Writing – review & editing. **David Shuster:** Conceptualization, Funding acquisition, Investigation, Methodology, Project administration, Supervision, Writing – review & editing.

Declaration of competing interest

The authors declare that they have no known competing financial interests or personal relationships that could have appeared to influence the work reported in this paper.

Data availability

All analytical data used in this study is included in this manuscript.

Acknowledgements

Appendix A. Supplementary material

Supplementary material related to this article can be found online at https://doi.org/10.1016/j.epsl.2022.117528.

References

Alley, R.B., Cuffey, K.M., Zoet, L.K., 2019. Glacial erosion: status and outlook. Ann. Glaciol. 60, 1–13.

Anderson, R.S., Molnar, P., Kessler, M.A., 2006. Features of glacial valley profiles simply explained. J. Geophys. Res., Earth Surf. 111.

Anderson, J.B., Warny, S., Askin, R.A., Wellner, J.S., Bohaty, S.M., Kirshner, A.E., Livsey, D.N., Simms, A.R., Smith, T.R., Ehrmann, W., Lawver, L.A., Barbeau, D., Wise, S.W., Kulhanek, D.K., Kulhenek, D.K., Weaver, F.M., Majewski, W., 2011. Progressive Cenozoic cooling and the demise of Antarctica's last refugium. Proc. Natl. Acad. Sci. USA 108, 11356–11360. https://doi.org/10.1073/pnas.1014885108.

Barker, P.F., Camerlenghi, A., 2002. Glacial history of the Antarctic Peninsula from Pacific margin sediments. In: Proceedings of the Ocean Drilling Program, Scientific Results. Ocean Drilling Program, College Station, Texas, USA, pp. 1–40.

Bart, P.J., Anderson, J.B., 2000. Relative temporal stability of the Antarctic ice sheets during the late Neogene based on the minimum frequency of outer shelf grounding events. Earth Planet. Sci. Lett. 182, 259–272.

Braun, J., 2003. Pecube: a new finite-element code to solve the 3D heat transport equation including the effects of a time-varying, finite amplitude surface topography. Comput. Geosci. 29, 787–794. https://doi.org/10.1016/S0098-3004(03)00052-9.

Breitsprecher, K., Thorkelson, D.J., 2009. Neogene kinematic history of Nazca-Antarctic-Phoenix slab windows beneath Patagonia and the Antarctic Peninsula. Tectonophysics 464, 10–20. https://doi.org/10.1016/j.tecto.2008.02.013.

Clinger, A.E., Fox, M., Balco, G., Cuffey, K., Shuster, D.L., 2020. Detrital thermochronometry reveals that the topography along the Antarctic Peninsula is not a Pleistocene landscape. J. Geophys. Res., Earth Surf., e2019JF005447. https://doi.org/10.1029/2019jf005447.

Cox, S.C., Smith Lyttle, B., the GeoMAP team, 2019. SCAR GeoMAP Dataset. GNS Science, Lower Hutt, New Zealand. Release v. 201907. https://doi.org/10.21420/7SH7-6K05.

Davies, B.J., Hambrey, M.J., Smellie, J.L., Carrivick, J.L., Glasser, N.F., 2012. Antarctic Peninsula Ice Sheet evolution during the Cenozoic Era. Quat. Sci. Rev. 31, 30–66. https://doi.org/10.1016/j.quascirev.2011.10.012.

Dühnforth, M., Anderson, R.S., Ward, D., Stock, G.M., 2010. Bedrock fracture control of glacial erosion processes and rates. Geology 38, 423–426.

Egholm, D.L., Nielsen, S.B., Pedersen, V.K., Lesemann, J.E., 2009. Glacial effects limiting mountain height. Nature 460, 884–887. https://doi.org/10.1038/nature08263.

Elliot, D.H., 1997. The planar crest of Graham Land, northern Antarctic Peninsula: possible origins and timing of uplift, vol. 71, pp. 51–73.

Farley, K.A., 2000. Helium diffusion from apatite: general behavior as illustrated by Durango fluorapatite. J. Geophys. Res. 105, 2903–2914. https://doi.org/10.1029/1999JB900348.

Flower, B.P., Kennett, J.P., 1994. The middle Miocene climatic transition: East Antarctic ice sheet development, deep ocean circulation and global carbon cycling. Palaeogeogr. Palaeoclimatol. Palaeoecol. 108, 537–555. https://doi.org/10.1016/0031-0182(94)90251-8.

Fox, M., 2019. A linear inverse method to reconstruct paleo-topography. Geomorphology 337, 151–164. https://doi.org/10.1016/j.geomorph.2019.03.034.

Furlong, K.P., Govers, R., 1999. Ephemeral crustal thickening at a triple junction: the Mendocino crustal conveyor. Geology 27, 127–130.

Guenthner, W.R., Barbeau, D.L., Reiners, P.W., Thomson, S.N., 2010. Slab window migration and terrane accretion preserved by low-temperature thermochronology of a magmatic arc, northern Antarctic Peninsula. Geochem. Geophys. Geosyst. 11, 1–13. https://doi.org/10.1029/2009GC002765.

Guillaume, B., Gautheron, C., Simon-Labric, T., Martinod, J., Roddaz, M., Douville, E., 2013. Dynamic topography control on Patagonian relief evolution as inferred from low temperature thermochronology. Earth Planet. Sci. Lett. 364, 157–167.

Haeuselmann, P., Granger, D.E., Jeannin, P.-Y., Lauritzen, S.-E., 2007. Abrupt glacial valley incision at 0.8 Ma dated from cave deposits in Switzerland. Geology 35, 143–146.

Herman, F., Seward, D., Valla, P.G., Carter, A., Kohn, B., Willett, S.D., Ehlers, T.A., 2013. Worldwide acceleration of mountain erosion under a cooling climate. Nature 504, 423–426. https://doi.org/10.1038/nature12877.

Huss, M., Farinotti, D., 2014. A high-resolution bedrock map for the Antarctic Peninsula. Cryosphere 8, 1261–1273. https://doi.org/10.5194/tc-8-1261-2014.

Jordan, T.A., Riley, T.R., Siddoway, C.S., 2020. The geological history and evolution of West Antarctica. Nat. Rev. Earth Environ. 1. https://doi.org/10.1038/s43017-019-0013-6.

Kessler, M.A., Anderson, R.S., Briner, J.P., 2008. Fjord insertion into continental margins driven by topographic steering of ice. Nat. Geosci. 1, 365–369. https://doi.org/10.1038/ngeo201.

Koppes, M., Hallet, B., Rignot, E., Mouginot, J., Wellner, J.S., Boldt, K., 2015. Observed latitudinal variations in erosion as a function of glacier dynamics. Nature 526, 100–103.

Koppes, M.N., Montgomery, D.R., 2009. The relative efficacy of fluvial and glacial erosion over modern to orogenic timescales. Nat. Geosci. 2, 644–647. https://doi.org/10.1038/ngeo616.

Larter, R.D., Barker, P.F., 1991. Effects of ridge crest-trench interaction on Antarctic-Phoenix spreading: forces on a young subducting plate. J. Geophys. Res., Solid Earth 96, 19583–19607.

Larter, R.D., Barker, P.F., 2009. Neogene interaction of tectonic and glacial processes at the Pacific margin of the Antarctic Peninsula. In: Sedimentation, Tectonics Eustasy Sea-Level Change. Act. Margins, p. 165.

Leith, K., Moore, J.R., Amann, F., Loew, S., 2014. Subglacial extensional fracture development and implications for Alpine Valley evolution. J. Geophys. Res., Earth Surf. 119, 62–81.

Molnar, P., Anderson, R.S., Anderson, S.P., 2007. Tectonics, fracturing of rock, and erosion. J. Geophys. Res., Earth Surf. 112.

Molnar, P., England, P., 1990. Late Cenozoic uplift: chicken or egg. Nature 346, 29–34. https://doi.org/10.1016/0021-9797(80)90501-9.

Müller, R.D., Cannon, J., Qin, X., Watson, R.J., Gurnis, M., Williams, S., Pfaffelmoser, T., Seton, M., Russell, S.H.J., Zahirovic, S., 2018. GPlates: building a virtual Earth through deep time. Geochem. Geophys. Geosyst. 19, 2243–2261.

Nesje, A., Whillans, I.M., 1994. Erosion of Sognefjord, Norway. Geomorphology 9, 33–45.

Oerlemans, J., 1984. Numerical experiments on glacial erosion. Z. Gletsch.kd. Glazialgeol. 20, 107–126.

Oerlemans, J., 2002. On glacial inception and orography. Quat. Int. 95, 5–10.

Osmundsen, P.T., Redfield, T.F., Hendriks, B.H.W., Bergh, S., Hansen, J., Henderson, I.H.C., Dehls, J., Lauknes, T.R., Larsen, Y., Anda, E., 2010. Fault-controlled alpine topography in Norway. J. Geol. Soc. (Lond.) 167, 83–98.

Pedersen, V.K., Egholm, D.L., 2013. Glaciations in response to climate variations preconditioned by evolving topography. Nature 493, 206–210.

Raymo, M.E., Ruddiman, W.F., 1992. Tectonic forcing of late Cenozoic climate. Nature 359, 117–122. https://doi.org/10.1038/359117a0.

Rebesco, M., Camerlenghi, A., Geletti, R., Canals, M., 2006. Margin architecture reveals the transition to the modern Antarctic ice sheet ca. 3 Ma. Geology 34, 301–304. https://doi.org/10.1130/G22000.1.

Rebesco, M., Larter, R.D., Barker, P.F., Camerlenghi, A., Vanneste, L.E., 1997. The history of sedimentation on the continental rise west of the Antarctic Peninsula. In: Geol. Seism. Stratigr. Antarct. Margin, 2, vol. 71, pp. 29–49.

Reiners, P.W., Brandon, M.T., 2006. Using thermochronology to understand orogenic erosion. Annu. Rev. Earth Planet. Sci. 34, 419–466.

Shuster, D.L., Cuffey, K.M., Sanders, J.W., Balco, G., 2011. Thermochronometry reveals headward propagation of erosion in an alpine landscape. Science 332, 84–88. https://doi.org/10.1126/science.1198401.

Smellie, J.L., Haywood, A.M., Hillenbrand, C.D., Lunt, D.J., Valdes, P.J., 2009. Nature of the Antarctic Peninsula Ice Sheet during the Pliocene: geological evidence and modelling results compared. Earth-Sci. Rev. 94, 79–94. https://doi.org/10.1016/j.earscirev.2009.03.005.

Spector, P., Balco, G., 2021. Exposure-age data from across Antarctica reveal mid-Miocene establishment of polar desert climate. Geology 49, 91–95.

Stevens Goddard, A.L., Fosdick, J.C., 2019. Multichronometer thermochronologic modeling of migrating spreading ridge subduction in southern Patagonia. Geology 47, e483. https://doi.org/10.1130/G46629C.1.

Tremblay, M.M., Fox, M., Schmidt, J.L., Tripathy-Lang, A., Wielicki, M.M., Harrison, T.M., Zeitler, P.K., Shuster, D.L., 2015. Erosion in southern Tibet shut down at ∼10 Ma due to enhanced rock uplift within the Himalaya. Proc. Natl. Acad. Sci. 112, 12030–12035. https://doi.org/10.1073/pnas.1515652112.

Turner, J., Lu, H., White, I., King, J.C., Phillips, T., Hosking, J.S., Bracegirdle, T.J., Marshall, G.J., Mulvaney, R., Deb, P., 2016. Absence of 21st century warming on Antarctic Peninsula consistent with natural variability. Nature 535, 411–415. https://doi.org/10.1038/nature18645.

Vaughan, A.P.M., Storey, B.C., 2000. The eastern Palmer Land shear zone: a new terrane accretion model for the Mesozoic development of the Antarctic Peninsula. J. Geol. Soc. (Lond.) 157, 1243–1256.

Willett, C.D., Ma, K.F., Brandon, M.T., Hourigan, J.K., Christeleit, E.C., Shuster, D.L., 2020. Transient glacial incision in the Patagonian Andes from ∼6 Ma to present. Sci. Adv. 6, 1–9. https://doi.org/10.1126/sciadv.aay1641.

Zachos, J., Pagani, H., Sloan, L., Thomas, E., Billups, K., 2001. Trends, rhythms, and aberrations in global climate 65 Ma to present. Science 292, 686–693. https://doi.org/10.1126/science.1059412.